Tribology Letters (2025) 73:8
https://doi.org/10.1007/s11249-024-01946-1

ORIGINAL PAPER

Effect of Humidity on the Wear Behavior of Graphene Under Current Carrying Conditions

Qian Tang[1] · Yuehua Huang[2] · Deen Sun[1] · Qunyang Li[3,4]

Received: 10 October 2024 / Accepted: 15 November 2024

Abstract
Wear problem has become an important issue limiting the functionality and lifetime of sliding electrical contact components. Adding conductive solid lubricants is a potential means of improving the tribological performance of these devices. Graphene, a two-dimensional material with excellent electrical conductivity and lubrication property, has been proposed to be a promising candidate for such applications. However, the tribological performance graphene has been demonstrated to be very susceptible to humidity even under non-current-carrying conditions. In this work, we study the effect of humidity on the wear behavior of graphene in the sliding electrical contact interfaces. The tribological behaviors of graphene under 10%, 30%, 60%, and 90% relative humidity conditions and 1 A current are investigated. The results show that the humidity can effectively slow down the wear of graphene in the sliding electrical contact interface by two key mechanisms. Firstly, as revealed by the infrared temperature measurements, higher humidity can significantly reduce the Joule heating. Secondly, X-ray photoelectron spectroscopy shows that with the existence of the electric current, at high humidity water molecules can passivate the graphene carbon dangling bonds more readily thereby reducing oxidation and slowing down the wear process. At low humidity, Joule heating not only caused graphene to oxidize but also accelerated the evaporation of water molecules, which was not conducive to its passivation, resulting in severe wear of the graphene.

Keywords Humidity · Graphene · Sliding electrical contact · Wear

1 Introduction

Sliding electrical contact components are extensively used in the areas of transport, electronics, machinery, and aerospace [1–4]. Various sliding electrical contact materials, such as precious metals, alloys, and composite materials, have good electrical conductivity, but their lifetime is short due to high friction and wear [5–8]. Wear problem has become an important issue limiting the functionality and lifetime of sliding electrical contact components. Adding conductive solid lubricants is a potential means of improving the tribological performance of these devices. Some materials such as graphite [9, 10], carbon fiber [11, 12], and molybdenum disulfide [13, 14] are effective in reducing friction and wear on the contact interface, but increase the contact resistance of the interface. Molybdenum disulfide can be only used in vacuum or dry conditions [15]. Thus, it is urgent to develop new conductive solid lubricants with excellent lubrication property and good conductivity for the friction interface.

Graphene, with excellent lubrication [16–20] and electrical properties [21–23], has been proposed to be a promising candidate for such applications. Diana Berman et al. investigate the feasibility of graphene as a conductive solid lubricant [24]. Graphene is sprayed on a gold-plated silicon substrate in the form of sporadic nanosheets, and the results show that graphene is effective in reducing friction and wear at current lower than 25 μA. Cao Z et al. investigate the sliding friction and current-carrying fretting behaviors of Ag/graphene composite coating in detail and Ag/graphene coating exhibits low friction coefficient

✉ Yuehua Huang
huangyuehua@swu.edu.cn

[1] Center for Advanced Thin Films and Devices, School of Materials and Energy, Southwest University, Chongqing 400715, China

[2] College of Engineering and Technology, Southwest University, Chongqing 400715, China

[3] Applied Mechanics Laboratory, Department of Engineering Mechanics, Tsinghua University, Beijing 100084, China

[4] Mechano-X Institute, Tsinghua University, Beijing 100084, China

Published online: 26 November 2024

and wear [25]. Our recent work demonstrates that graphene provides stable lubrication and conductivity on brass/copper in various test methods and test parameters [26]. Apparently, graphene is feasible as a conductive solid lubricant.

It is well known that the lubrication property of graphite is environmentally sensitive [27, 28]. Graphene, the basic unit of graphite, is also very sensitive to the environment humidity [29, 30]. Over the past few years, researchers have demonstrated that humidity has a significant effect on the wear behavior of graphene [31–34]. Bhowmick et al. find that the friction coefficient of graphene in dry nitrogen atmosphere is about 0.52 and reduces to 0.17 in 10% relative humidity (RH), which further decreases with increasing humidity [32]. The wear degree of graphene also decreases with the increase of humidity. The authors attribute the phenomenon to the passivation of carbon dangling bonds at the graphene defects by H and OH, which are decomposed by water molecules. Li et al. demonstrate the durability of graphene at 90% RH is longer than that in the nitrogen atmosphere and they also attribute the phenomenon to the passivation of graphene by water [33]. Previous research in our group also confirms that humidity significantly slows down the wear of monolayer graphene [34]. However, the effect of humidity on the wear behavior of graphene under current carrying conditions has not been investigated.

Recently, we demonstrate that graphene has good lubrication properties and good electrical conductivity on copper/brass [26]. Our previous work also proves that humidity can significantly slow down the wear of graphene under non-current conditions [34]. In this work, we further study the influence of humidity on the wear behavior of graphene under current carrying conditions and the underlying mechanism. The results demonstrates that the humidity significantly slows down the wear of graphene under current carrying conditions. We combine temperature measurement by infrared imager and X-ray photoelectron spectroscopy to explore the underlying mechanism. Firstly, sliding experiments show that the wear of graphene and brass substrate is more serious when there is a current in the sliding contact interface. We think this is mainly due to that the Joule heating promotes the oxidation of graphene and brass substrate. The temperature of sliding counterparts and the contact resistance of the sliding interface under relative high humidity environment are both lower than those in lower humidity environment, which demonstrate the humidity slows down the wear of graphene by reducing the Joule heating. Secondly, the X-ray photoelectron spectroscopy results of the graphene debris in the wear tracks indicate that water molecules can passivate graphene carbon dangling bonds under current carrying conditions, thus significantly reduce the oxidation of graphene and thereby slow down its wear.

2 Material and Methods

The graphene aqueous solution was purchased from Beijing Dk Nanotechnology (Beijing, China), and it is prepared by a modified Hummers method. 5 mg/mL graphene solution was uniformly applied to the brass surface (15 mm*15 mm) and dried at 30 ℃. A current-carrying tribometer (MS-M9000, Lanzhou Huahui Instrument Technology Co., Ltd, China) was used, and 6 mm steel balls were used as the friction pair. The normal load was 1N, the sliding frequency was 2 Hz, the reciprocating sliding distance was 5 mm and the testing cycle was 3000 cycles. The current was between 0.1 A and 2 A. The humidity of the test environments was 10%, 30%, 60%, and 90%, respectively. The humidity control methods were as follows: firstly, the dry nitrogen (N_2) was divided into two parts, one part through the water to become wet nitrogen, the other part is not treated. Then regulated the wet N_2 and dry N_2 ratios to control the test chamber's humidity, as shown in Fig. S1. The hygrometer (Rotronic, HygroLog HL-NT3) was placed in the test atmosphere chamber next to the friction counterpart to monitor the humidity of the test chamber, as shown in Fig. S1.

The temperature of the sliding counterparts was measured by an infrared thermal imager (FLUKE, TiX875). The wear tracks were analyzed by optical microscopy (LEICA, DM2700M), Raman spectra (HORIBA, XploRA PLUS010410), X-ray photoelectron spectra (XPS, PHI Quantera II) and a probe surface profiler (Bruker, DektakXT).

3 Results and Discussion

The friction measurement schematic diagram is exhibits in Fig. 1a. The device inputs a constant current while measuring the voltage drop to obtain the contact resistance of the friction interface. The device simultaneously collects the friction force and the electrical signal of the sliding electrical contact interface. Graphene is evenly distributed on the brass substrate before test, as shown in Fig. 1b. Figure 1c shows the Raman spectrum of graphene at the red spot in (b). The D, G, and 2D peaks of graphene can be observed. The D peak at 1350 cm^{-1} indicates the defect of graphene as well as the degree of disorder. The G peak at 1580 cm^{-1} indicates the integrity of graphene. The intensity of the G peak is much higher than that of the D peak, indicating the integrity of the graphene is high.

The tribological behaviors of graphene with 1 A under 10% RH, 30% RH, 60% RH, and 90% RH are investigated, as exhibited in Fig. 2. The friction coefficient of graphene

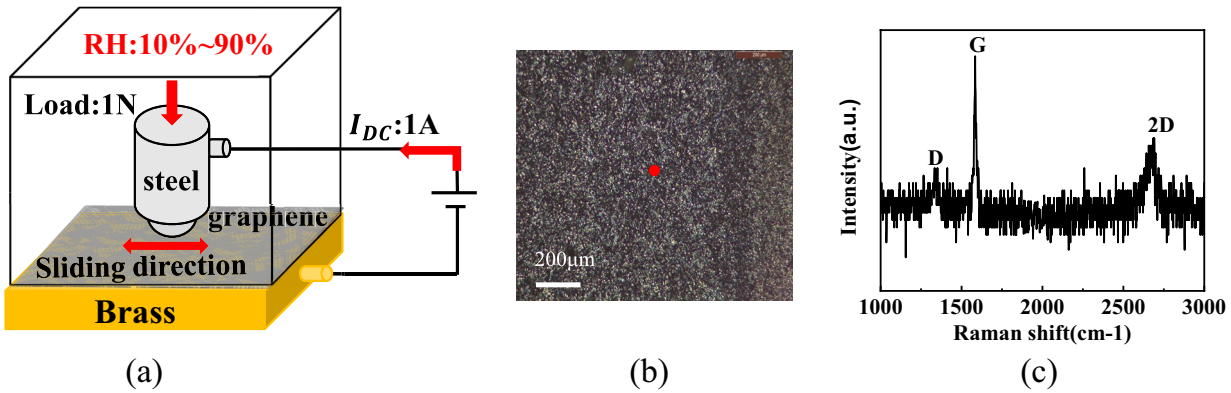

Fig. 1 **a** The schematic diagram with different humidity for the graphene film/steel ball friction interface; **b** Optical microscope images of graphene deposited on the brass; **c** Raman spectrum of the red spot in (**b**)

Fig. 2 Effect of humidity on the tribological behavior of graphene under current carrying conditions. **a** Friction coefficient under different humidity with 1 A; **b** Contact resistance under different humidity with 1 A; **c** Optical microscope images of the wear tracks; **d** The height profiles along the white lines in the wear tracks in (**c**); **e** The Raman spectra of the white spots in the wear tracks in (**c**)

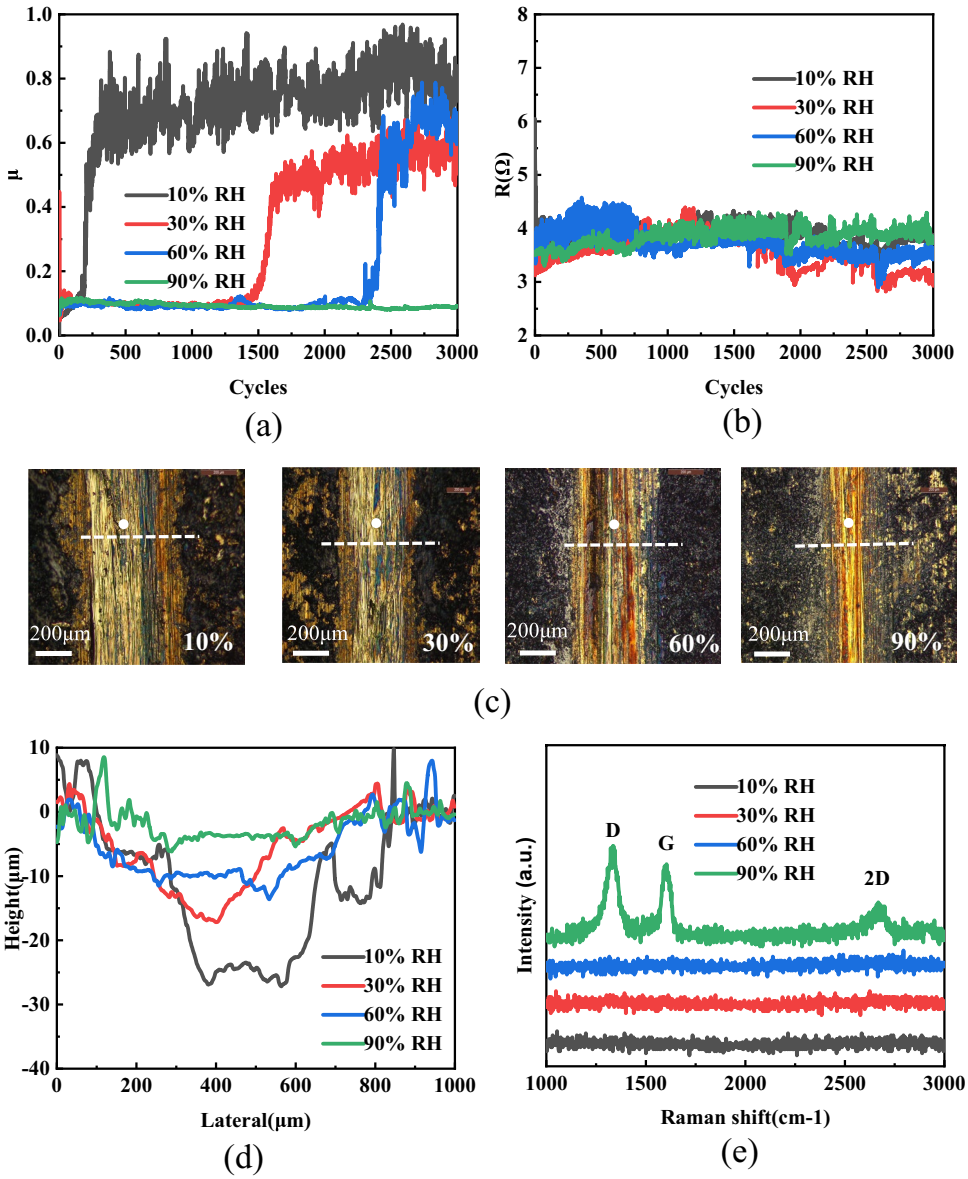

at different humidity before failure is about 0.1, which rapidly increases to 0.6–0.8 and remains stable after destruction or removal of the graphene film during reciprocating sliding (The friction coefficient without graphene is about 0.7, as shown in Fig. S2(a)). The presence of gas molecules on the surface of graphene can affect the friction coefficient at high humidity conditions. The friction coefficients of graphene before failure under different humidity conditions are basically the same. Thus, we speculate that there are no liquid water molecules on the graphene surface at high humidity. The low friction duration under different humidity conditions is different. The low friction lasts for 170 cycles, 1420 cycles and 2300 cycles when the humidity is 10%, 30% and 60%, respectively. When the humidity further increases to 90%, the low friction coefficient is maintained during the whole sliding test. Moreover, the friction coefficient before graphene failure under different humidity conditions is different. Figure 2b shows the corresponding contact resistance during sliding, which is relatively stable during sliding, basically at 3–4 Ω. Based on the results in Fig. 2a, b, we believe there is no necessary connection between the coefficient of friction and the contact resistance. As shown in Fig. S3, the friction coefficient of the Steel/Brass friction interface is high without graphene and is low with graphene. Due to the good conductivity of graphene, the contact resistance of the Steel/Brass friction interface is both low with and without graphene. After the friction, we test the wear tracks at 3000 cycles. The optical microscopy images of the wear tracks under different humidity conditions are displayed in Fig. 2c. The width of the corresponding wear tracks is 734 μm, 695 μm and 586 μm when the humidity is 10%, 30% and 60%, respectively. In addition, there is almost no graphene in the wear tracks. While the humidity is 90%, the width of the wear track is 348 μm. Meanwhile, there is some graphene debris in the wear track (the enlarged image is shown in Fig. S4). With the increase of humidity, the wear track width gradually increases. Figure 3d exhibits the height profiles of wear tracks corresponding to the white line in Fig. 3c. The wear tracks depth is 26 μm, 15 μm, 8 μm, 4 μm when the humidity is 10%, 30%,60% and 90%, respectively. Figure 2e) shows the Raman spectra at the white spot in the wear track in (c). There are no obvious peaks in the Raman spectra of spots under 10% RH, 30% RH and 60% RH, demonstrating that graphene failure. This is consistent with the friction coefficient variation in Fig. 2a. When the humidity increases to 90%, the characteristic peaks of graphene D, G, and 2D peaks are observed in the Raman spectrum, demonstrating the presence of graphene in the wear track and continues to have a lubricating effect. This is consistent with the friction coefficient variation in Fig. 2a. The D peak appears, indicating the increase of disorder and defects in the graphene during the electrical sliding test. In the case of current, increasing humidity can effectively slow down the wear of graphene.

Figure 3 shows the friction test with 0 A and 1 A in ambient environment and the temperature variations of the sliding contact interfaces are simultaneously recorded using an infrared thermographic camera. The coefficient of friction evolution curves at 0 A and 1 A in ambient environment are exhibited in Fig. 3a. The coefficient of friction is approximately 0.05 at 0 A and remains stable during the sliding test. The coefficient of friction under 1 A remains stable at 0.1 around and increases to 0.55 at 1700 cycles. Figure 3b exhibits the optical microscopic image of the wear tracks and their corresponding height profile. The width of the wear track without current is 383 μm. Meanwhile, the graphene debris can be seen in the wear track (the enlarged image is shown in Fig. S5). From the height profile, the depth of the wear track without current is 6 μm. In contrast, the width and depth of the wear track under 1 A is 620 μm and 15 μm, respectively. The wear track under 1 A is obviously wider and deeper. The Raman spectra of the white spots in the wear tracks in (b) are shown in Fig. 3c. When there is no current, only the G peak appears in graphene, and the integrity of graphene is close to that of the original graphene. There is no obvious peak under 1 A, indicating that graphene is severely destroyed or removed during the test. The Raman results further demonstrate that the wear is serious when the current is present. Figure 3d exhibits the temperature variation of a spot on the friction pair marked by the white spot in Fig. 3e during the friction test under 0 A and 1 A. The temperature of the spot on the friction pair before sliding test is 16 °C. In the case of non-current, the temperature of the spot on the friction pair has no obvious variation and maintains at about 16 °C. However, the temperature of the spot on the friction pair under 1 A increases rapidly from 16 to 20 °C. Thereafter, it slowly increases to 22 °C and remains stable. At 1700 cycles, the temperature slowly decreases to about 20 °C until the end of the test and it is consistent with the decrease of friction coefficient at 1700 cycles in Fig. 3a, both of which are due to the failure of the graphene and the exposure of the brass substrate. Under 1 A conditions, the temperature decreases at 1700 cycles due to the exposure of the brass substrate, which accelerates heat dissipation. Figure 3e exhibits the infrared images during the friction test in the 0th, 600th, 1200th, 2400th and 3000th cycles. The temperature scale for each infrared image is different. In order to better show the temperature variation of the steel/brass interface, we put a local enlarged image of the contact interface. It can be generally observed that the temperature of the friction pair remains basically stable when there is no current. However, when 1 A current is inputted, the temperature of friction pair first increases, then decreases and remains stable at last. The whole temperature change process

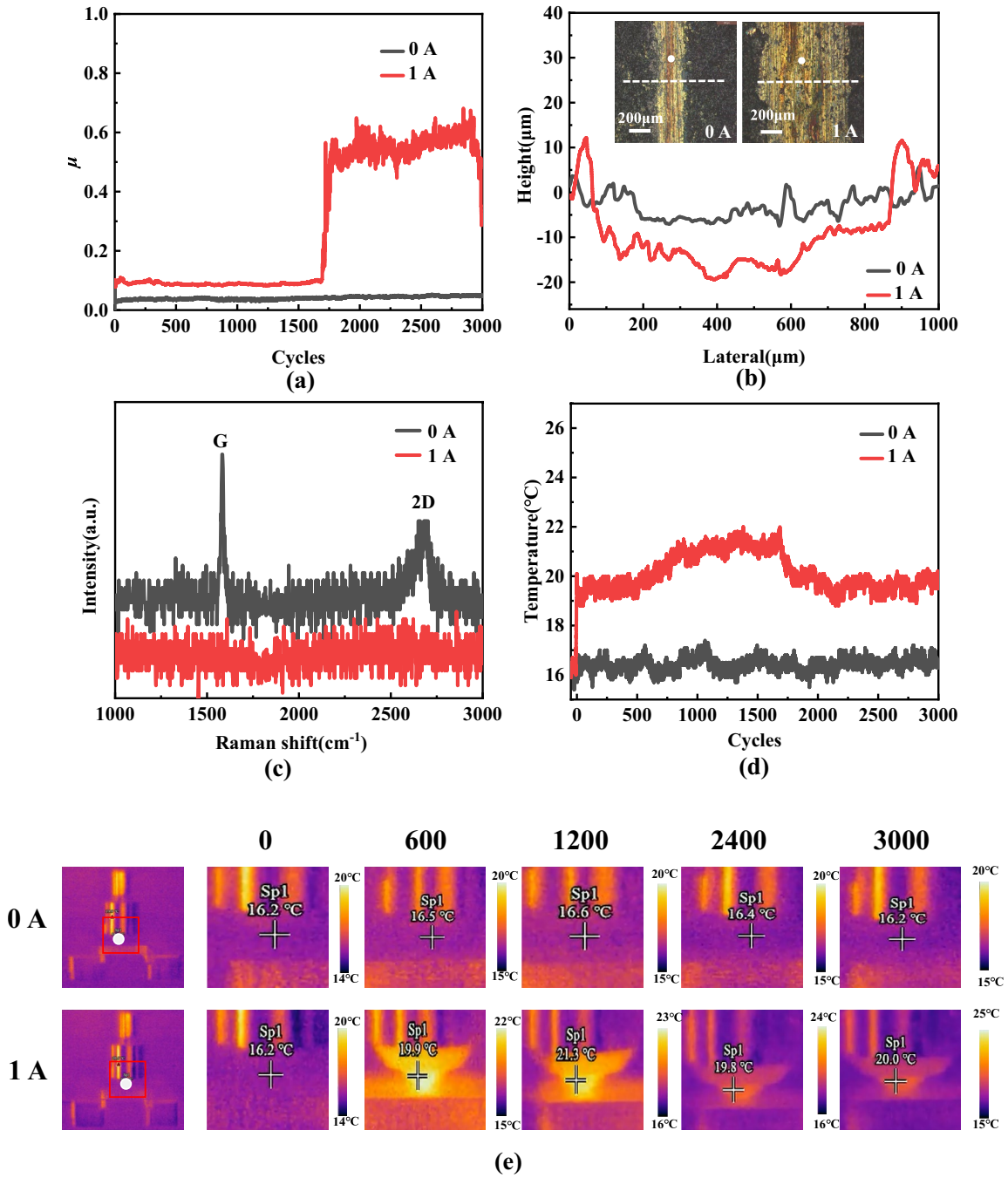

Fig. 3 Influence of electric current on the tribological behavior of graphene. **a** Friction coefficients under 0 A and 1 A in ambient environment; **b** The optical microscope images of wear tracks and the corresponding height profiles as labeled with white lines; **c** Raman spectra of the white spots in the wear track in (**b**); **d** The temperature variation of the spot on the friction pair marked by the white point in (**e**); **e** The corresponding infrared images of the sliding electrical contact interfaces at different cycles with 0 A and 1 A in (**a**)

under 0 A and 1 A conditions is shown in Movie S1 and Movie S2, respectively. Figure 3 demonstrates that the Joule heating generated by the current is significantly higher than the frictional heat. Microscopic experiments have confirmed that Joule heating caused by electric current will reduce the mechanical strength of graphene and cause its destruction [35]. Joule heating can cause serious oxidation and wear of copper and its alloys [36, 37]. Therefore, we think the Joule heating generated by the current promotes the oxidation of graphene and brass substrate, resulting in more severe wear of graphene.

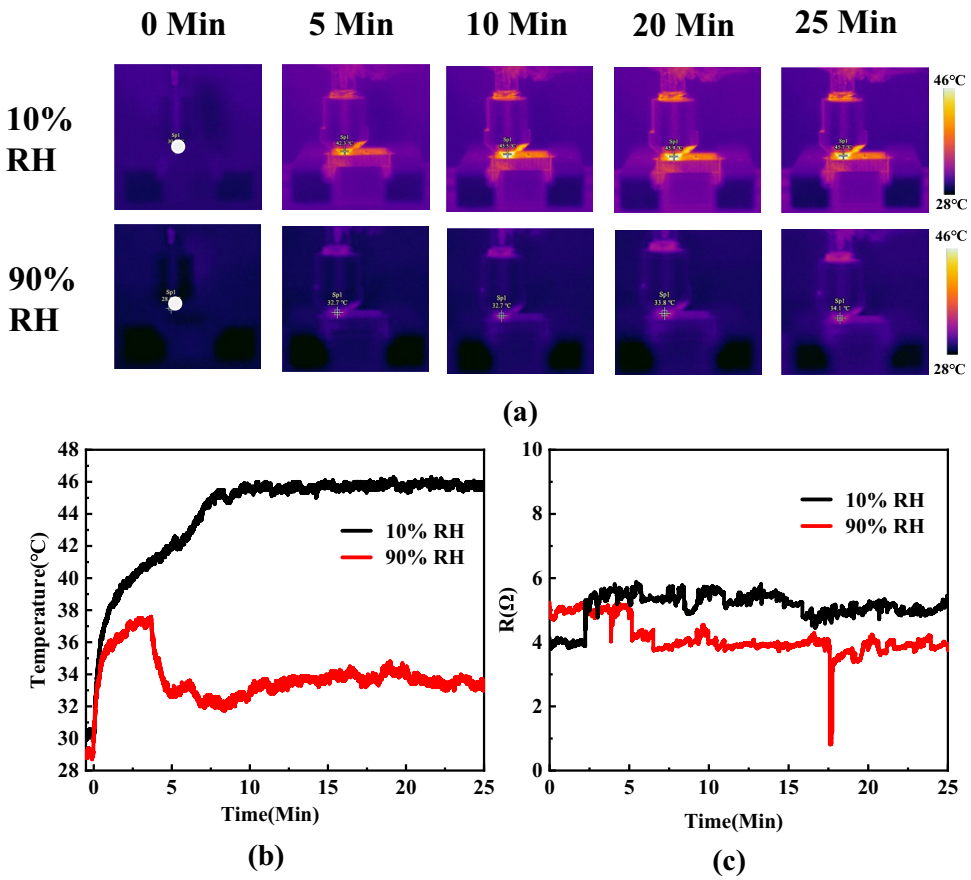

Fig. 4 Effect of humidity on the Joule heating. **a** The infrared images of the steel/graphene contact interface in 10% RH and 90% RH environments under 1 A current with the increase of time; **b** The temperature variation of the white spot on the steel ball in (**a**) with the increase of time; **c** The contact resistance of the steel/graphene contact interface in 10% RH and 90% RH environments under 1 A current with the increase of time

Figure 4 investigates the influence of humidity on the Joule heating by recording the temperature variation of the steel/graphene contact interface in 10% RH and 90% RH environments under 1 A current with the increase of time by the infrared thermographic camera. Figure 4a displays the infrared images of the contact interface in the 0th, 5th, 10th, 20th and 25th minutes and the whole temperature change process under 10% RH and 90% RH environments is shown in Movie S3 and Movie S4, respectively. It can be observed that the temperature of the steel ball under 1 A at 10% RH is obviously higher than that at 90% RH. To make a more accurate comparison, the temperature variations of the white spot on the steel ball in Fig. 4a in 10% RH and 90% RH environments under 1 A current with the increase of time are plotted in Fig. 4b. Under 10% RH, the temperature of the spot on steel ball abruptly increases from 30.5 to 35 ℃ during the first two seconds, and gradually increases to 45.5 ℃ in the tenth minute, and then remains stable at around 45.5 ℃ at the end of the test. Under 90% RH, the temperature of the spot on steel ball increases rapidly from 28.8 to 35 °C in the first two seconds and then gradually increases to 37 ℃ in the fourth minute. In the fifth minute, it drops to 32.7 ℃ and then fluctuates between 32 and 35 ℃. It demonstrates that the temperature rise of the friction pair in a dry condition is higher than that of the friction pair in a wet condition. The contact resistances are tested simultaneously, as exhibited in Fig. 4c. The contact resistance of the steel/graphene contact interface is about 4 Ω under 90% RH conditions and about 5 Ω under 10% RH conditions. For the same current and duration, according to $Q = I^2Rt$, more Joule heating is produced by the current in a dry environment, which is consistent with the result of Fig. 4b. In summary, at humidity environment, water molecules can effectively reduce the Joule heating.

Based on the results in Figs. 3 and 4, we believe that the Joule heating caused by the current accelerates the oxidation of graphene and copper substrate and thus speeds up the wear of graphene. While the high humidity can obviously reduce the Joule heating and slow down the wear of graphene.

In addition to the infrared temperature measurement, which reveals that the humidity reduces Joule heating and thus slows down the wear of graphene, we further analyze the molecular structure and chemical bonds of graphene debris at the wear scars at sliding electrical interface by XPS. For comparison, graphene debris at wear tracks in 90% RH and 10% RH in 1 A are selected as analysis objects. Since there is no graphene debris in the wear track in 10% RH, 1 A condition, as shown in the Raman spectrum in Fig. 2e, we test graphene debris at the wear track under

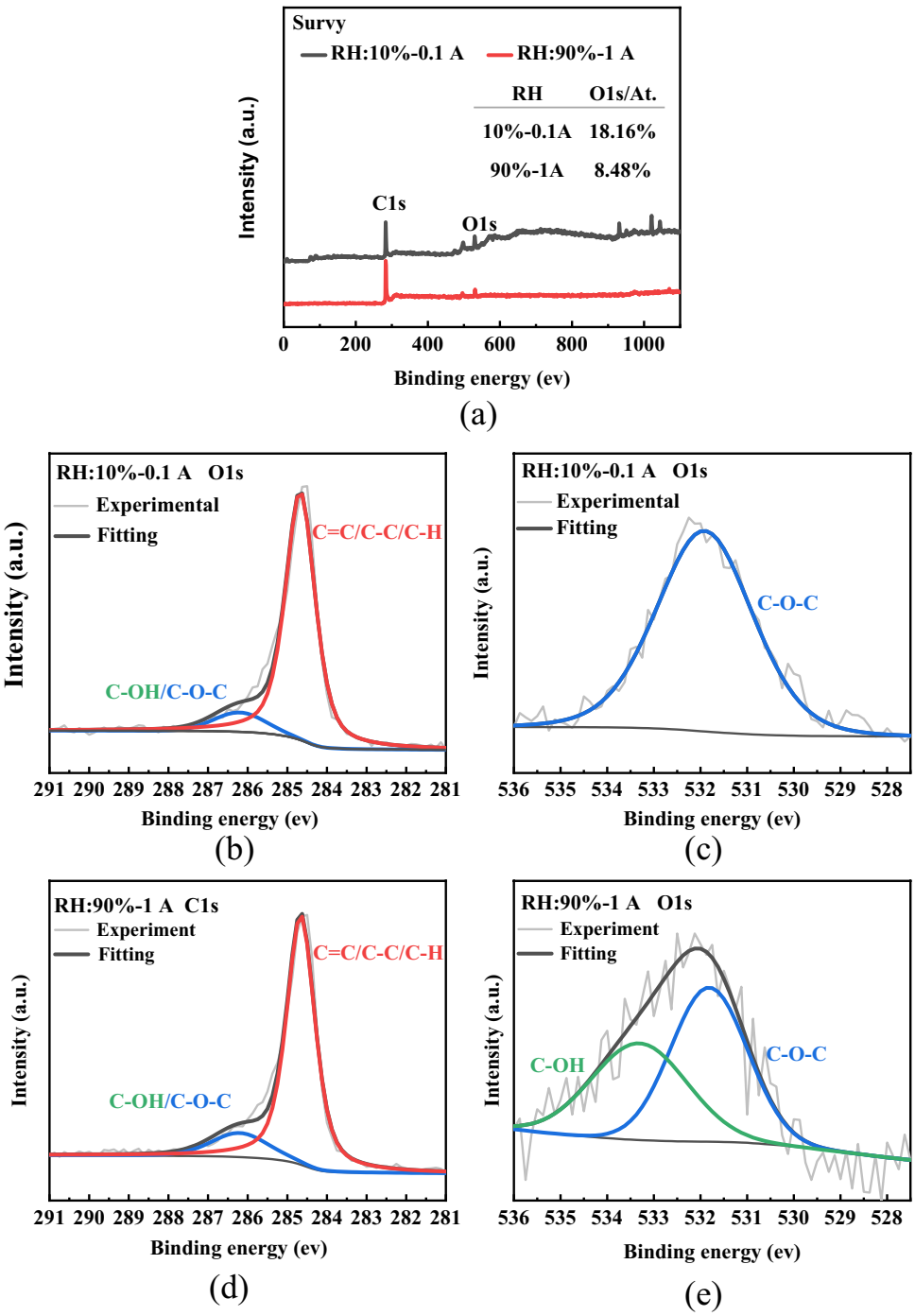

Fig. 5 **a** XPS spectra of the graphene debris in the wear tracks with 10% RH, 0.1 A and 90% RH, 1 A, the inset table is the corresponding calculated oxygen content; **b** the C1s and b the O1s XPS spectrum of the graphene debris in the wear track with 10% RH, 0.1 A; **d** the C1s and **e** the O1s XPS spectrum of the graphene debris in the wear track with 90% RH, 1 A

10% RH, 0.1 A as an alternative comparison, whose Raman spectrum is shown in Fig. S6. XPS spectra of the graphene debris in the wear tracks with 10% RH, 0.1 A, and 90% RH, 1 A are shown in Fig. 5a. The oxygen atom fraction is obtained by comparing the peak area of C1s and O1s. The fraction of oxygen atoms is around 18.16% at 10% RH, 0.1 A and around 8.48% at 90% RH, 1 A, indicating that the oxidation degree of graphene in 90% RH is less than that in 10% RH. This is consistent with the result of the friction test in Fig. 2a and the Raman result in Fig. 2e. The C1s and O1s spectra of graphene debris in the wear tracks are further analyzed. The raw and fitted C1s and O1s spectra of graphene at 10% RH, 0.1 A are shown in Fig. 5b, c, respectively. Figure 5d, e present the raw and fitted C1s and O1s spectra at 90% RH, 1 A, respectively. The binding energy of the sp^2 C–C bonding (red) is assigned at 284.6 eV and 286.3 eV (blue) is assigned for C–OH/C–O–C [32, 33, 38]. The binding energy of the C–O–C bonding (blue) is assigned

at 531.8 eV and 533.6 eV (green) is assigned for C–OH [38, 39]. In C1s spectra in Fig. 5b, d, peak corresponding to C–OH/C–O–C (blue) can be clearly identified, indicating the oxidation or passivation of graphene. The spectra of C1s are basically the same in both conditions. However, there are significant differences in the spectra of O1s in different RH conditions. In the spectrum with 10% RH, 0.1 A, only the O1s peak appears at a binding energy of 531.8 eV, which is attributed to O–C–O. While peaks corresponding to O–C–O (531.8 eV, blue) and C–OH (533.6 eV, green) can be clearly identified in the O1s spectrum with 90% RH,1 A. This C–OH peak with 90% RH, 1 A condition indicates the passivating effect of water on carbon dangling bonds. The XPS results confirm that at high humidity, water molecules passivate carbon dangling bonds in graphene at sliding electrical contact interfaces, thus effectively reducing the oxidation of graphene and thereby slowing down wear. Whereas at low humidity, there is no significant passivation effect, which may be due to joule heating causing water molecules to evaporate rapidly.

4 Conclusions

In this work, we studied the influence of humidity on the wear behavior of graphene under current carrying conditions. Experiments demonstrated that water molecules can significantly slow down the wear of graphene under current carrying conditions. We used infrared temperature measurement and XPS component analysis to explore the underlying mechanism. Firstly, the current would accelerate the wear of graphene, which we believed was due to that the Joule heating accelerated the oxidation of graphene and the brass substrate. While infrared experiments confirmed that water molecules could reduce the Joule heating, resulting in slowing down the wear of graphene. Secondly, the XPS results indicated that even in the existence of current, water molecules could passivate the carbon dangling bond on the surface of graphene. At high humidity, the passivation effect of water molecules was significant, which could effectively inhibit the oxidation of graphene, thereby slowing down graphene wear. At low humidity, Joule heating led to significant wear of the graphene since it not only oxidized the material but also hastened the evaporation of water molecules, which was detrimental to its passivation. Our study revealed the influence and mechanism of humidity on the wear behavior of graphene under current carrying conditions and provided a reference for related research and practical application of graphene under current carrying conditions.

Supplementary Information The online version contains supplementary material available at https://doi.org/10.1007/s11249-024-01946-1.

Author Contributions Tang: Data curation, Formal analysis, Writing-original draft. Yuehua Huang: Investigation, Supervision, Writing-review and editing. Deen Sun: Resources. Qunyang Li: Writing-review and editing. The manuscript was accomplished through contributions of all authors. All authors have given approval to the manuscript.

Funding The work was financially supported by the National Natural Science Foundation of China (Nos. 12302127, 12025203).

Data Availability No datasets were generated or analysed during the current study.

Declarations

Conflict of interest The authors declare no competing interests.

References

1. Kloch, K.T., Kozak, P., Mlyniec, A.: A review and perspectives on predicting the performance and durability of electrical contacts in automotive applications. Eng. Fail. Anal. **121**, 105143 (2021). https://doi.org/10.1016/j.engfailanal.2020.105143
2. Yang, Y., Pei, L., Zhang, H., Feng, K., Ju, P., Duan, W., et al.: Magnetron sputtering NbSe2 film as lubricant for space current-carrying sliding contact. Friction **11**, 383–394 (2022). https://doi.org/10.1007/S40544-022-0603-Z
3. Calderon-Salmeron, G., Leckner, J., Westbroek, R., Chanamolu, B., Glavatskih, S.: Greases for electric vehicle motors: bearing friction torque under driving cycle conditions and the thickener effect on oil release. Tribol. Int. **198**, 109777 (2024). https://doi.org/10.1016/j.triboint.2024.109777
4. Yang, Z., Song, Y., Jiao, J., Li, W., Shangguan, B., Zhang, Y.: Optimization of current-carrying friction and wear properties of copper-carbon composite materials based on damage. Tribol. Int. **191**, 109074 (2024). https://doi.org/10.1016/j.triboint.2023.109074
5. Mei, G., Fu, W., Chen, G., Zhang, W.: Effect of high-density current on the wear of carbon sliders against Cu–Ag wires. Wear **452–453**, 203275 (2020). https://doi.org/10.1016/j.wear.2020.203275
6. Kubota, Y., Nagasaka, S., Miyauchi, T., Yamashita, C., Kakishima, H.: Sliding wear behavior of copper alloy impregnated C/C composites under an electrical current. Wear **302**, 1492–1498 (2013). https://doi.org/10.1016/j.wear.2012.11.029
7. Argibay, N., Bares, J.A., Sawyer, W.G.: Asymmetric wear behavior of self-mated copper fiber brush and slip-ring sliding electrical contacts in a humid carbon dioxide environment. Wear **268**, 455–463 (2010). https://doi.org/10.1016/j.wear.2009.08.036
8. Wang, P., Zhang, H., Yin, J., Xiong, X., Tan, C., Deng, C., et al.: Wear and friction behaviours of copper mesh and flaky graphite-modified carbon/carbon composite for sliding contact material under electric current. Wear **380–381**, 59–65 (2017). https://doi.org/10.1016/j.wear.2017.02.045
9. Bares, J.A., Argibay, N., Dickrell, P.L., Bourne, G.R., Burris, D.L., Ziegert, J.C., et al.: In situ graphite lubrication of metallic sliding electrical contacts. Wear **267**, 1462–1469 (2009). https://doi.org/10.1016/j.wear.2009.03.024
10. Zhao, J., Li, Y., Liu, Y., Huang, W., Xu, Y.: Friction and wear performances of impregnated graphite in ring-on-ring tribological test. Tribol. Int. **174**, 107715 (2022). https://doi.org/10.1016/j.triboint.2022.107715
11. Lin, L., Schlarb, A.K.: Recycled carbon fibers as reinforcements for hybrid PEEK composites with excellent friction and wear

performance. Wear **432–433**, 202929 (2019). https://doi.org/10.1016/j.wear.2019.202928
12. Mao, L., Jiao, Y., Geng, H., Tang, Y.: Understanding friction and wear properties of carbon fiber/epoxy stitched composites. Compos. Part A **169**, 107501 (2023). https://doi.org/10.1016/j.compositesa.2023.107501
13. Kumari, S., Mungse, H.P., Gusain, R., Kumar, N., Sugimura, H., Khatri, O.P.: Octadecanethiol-grafted molybdenum disulfide nanosheets as oil-dispersible additive for reduction of friction and wear. FlatChem **3**, 16–25 (2017). https://doi.org/10.1016/j.flatc.2017.06.004
14. Mutyala, K.C., Wu, Y.A., Erdemir, A., Sumant, A.V.: Graphene—MoS2 ensembles to reduce friction and wear in DLC-Steel contacts. Carbon **146**, 524–527 (2019). https://doi.org/10.1016/j.carbon.2019.02.047
15. Ju, H., Wang, R., Ding, N., Yu, L., Xu, J., Ahmed, F., et al.: Improvement on the oxidation resistance and tribological properties of molybdenum disulfide film by doping nitrogen. Mater. Des. **186**, 108300 (2020). https://doi.org/10.1016/j.matdes.2019.108300
16. Berman, D., Erdemir, A., Sumant, A.V.: Graphene: a new emerging lubricant. Mater. Today **17**, 31–42 (2014). https://doi.org/10.1016/j.mattod.2013.12.003
17. Klemenz, A., Pastewka, L., Balakrishna, S.G., Caron, A., Bennewitz, R., Moseler, M.: Atomic scale mechanisms of friction reduction and wear protection by graphene. Nano Lett. **14**, 7145–7152 (2014). https://doi.org/10.1021/nl5037403
18. Restuccia, P., Righi, M.C.: Tribochemistry of graphene on iron and its possible role in lubrication of steel. Carbon **106**, 118–124 (2016). https://doi.org/10.1016/j.carbon.2016.05.025
19. Huang, Y., Li, Q., Zhang, J., Qi, Y., Wang, H., Zhao, P., et al.: Effect of airborne contaminants on the macroscopic anti-wear performance of chemical vapor deposition graphene. Surf. Coat. Technol. **383**, 125276 (2020). https://doi.org/10.1016/j.surfcoat.2019.125276
20. Huang, Y., Li, Q., Zhang, J., Wang, H., Zhao, P., Meng, Y.: Electric resistance as a sensitive measure for detecting graphene wear during macroscale tribological tests. Sci. China Technol. Sci. **64**, 179–186 (2020). https://doi.org/10.1007/s11431-020-1631-4
21. Huang, Y., Xiang, Y., Ren, W., Li, F., Li, C., Yang, T.: Enhancing the sensitivity of crack-based strain sensor assembled by functionalized graphene for human motion detection. Sci. China Technol. Sci. **64**, 1805–1813 (2021). https://doi.org/10.1007/s11431-021-1856-6
22. Li, J., Liao, Z., Liang, T., Zhang, S., Tang, B., Fu, X., et al.: High sensitivity, fast response and anti-interference crack-based reduced graphene oxide strain sensor for pig acoustic recognition. Comput. Electron. Agric. **200**, 107267 (2022). https://doi.org/10.1016/j.compag.2022.107267
23. Huang, Y., Zeng, Z., Liang, T., Li, J., Liao, Z., Li, J., et al.: An encapsulation strategy of graphene humidity sensor for enhanced anti-interference ability. Sens. Actuators B **396**, 134517 (2023). https://doi.org/10.1016/j.snb.2023.134517
24. Berman, D., Erdemir, A., Sumant, A.V.: Graphene as a protective coating and superior lubricant for electrical contacts. Appl. Phys. Lett. **105**, 231907 (2014). https://doi.org/10.1063/1.4903933
25. Cao, Z., Li, R., Shou, M., Luo, R., Wei, B., Wang, T.: Mechanical properties and tribological behaviors of Ag/graphene composite coating under sliding friction and current-carrying fretting. Tribol. Int. **197**, 109811 (2024). https://doi.org/10.1016/j.triboint.2024.109811
26. Wang, L., Tang, Q., Liang, T., Liu, C., Sun, D., Wang, S., et al.: Lubrication performance of graphene in the sliding electrical contact interface. Friction (2024). https://doi.org/10.1007/s40544-024-0910-7
27. Ling, T.Y., Pu, S.H., Fishlock, S.J., Han, Y., Reynolds, J.D., McBride, J.W., et al.: Sensing performance of nanocrystalline graphite-based humidity sensors. IEEE Sens. J. **19**, 5421–5428 (2019). https://doi.org/10.1109/isen.2019.2905719
28. Tahir, N.A.M., Liza, S., Fukuda, K., Yaakob, Y., Zulkifli, N.A., Rawian, N.A.M., et al.: Influence of humidity on the tribological performance of graphite reinforced aluminium anodic oxide coating. Tribol. Int. **197**, 109752 (2024). https://doi.org/10.1016/j.triboint.2024.109752
29. Fong, K.C., Schwab, K.C.: Ultrasensitive and wide-bandwidth thermal measurements of graphene at low temperatures. Phys. Rev. X **2**, 031006 (2012). https://doi.org/10.1103/physrevx.2.031006
30. Xiao, X., Li, C., Fan, S.-C., Liu, Y.-J., Liu, Y.: Optical-thermally actuated graphene mechanical resonator for humidity sensing. Sens. Actuators B **374**, 132851 (2023). https://doi.org/10.1016/j.snb.2022.132851
31. Gao, X., Chen, L., Ji, L., Liu, X., Li, H., Zhou, H., et al.: Humidity-sensitive macroscopic lubrication behavior of an as-sprayed graphene oxide coating. Carbon **140**, 124–130 (2018). https://doi.org/10.1016/j.carbon.2018.08.035
32. Bhowmick, S., Banerji, A., Alpas, A.T.: Role of humidity in reducing sliding friction of multilayered graphene. Carbon **87**, 374–384 (2015). https://doi.org/10.1016/j.carbon.2015.01.053
33. Li, Z.-Y., Yang, W.-J., Wu, Y.-P., Wu, S.-B., Cai, Z.-B.: Role of humidity in reducing the friction of graphene layers on textured surfaces. Appl. Surf. Sci. **403**, 362–370 (2017). https://doi.org/10.1016/j.apsusc.2017.01.226
34. Huang, Y., Yao, Q., Qi, Y., Cheng, Y., Wang, H., Li, Q., et al.: Wear evolution of monolayer graphene at the macroscale. Carbon **115**, 600–607 (2017). https://doi.org/10.1016/j.carbon.2017.01.056
35. Huang, P., Guo, D., Xie, G., Li, J.: Softened mechanical properties of graphene induced by electric field. Nano Lett. **17**, 6280–6286 (2017). https://doi.org/10.1021/acs.nanolett.7b02965
36. Sun, Y., Song, C., Liu, Z., Li, J., Wang, L., Sun, C., Zhang, Y.: Tribological and conductive behavior of Cu/Cu rolling current-carrying pairs in a water environment. Tribol. Int. **143**, 106055 (2020). https://doi.org/10.1016/j.triboint.2019.106055
37. Hu, Z.L., Chen, Z.H., Xia, J.T.: Study on surface film in the wear of electrographite brushes against copper commutators for variable current and humidity. Wear **264**, 11–17 (2008). https://doi.org/10.1016/j.wear.2007.01.034
38. Lang, H., Peng, Y., Shao, G., Zou, K., Tao, G.: Dual control of the nanofriction of graphene. J. Mater. Chem. C **7**, 6041–6051 (2019). https://doi.org/10.1039/c9tc01148j
39. Sun, Y., Li, J., Yang, H., Kang, X., Zhang, L.: Effect of electric current on the microstructural evolution and tribological behavior of highly oriented pyrolytic graphite. J. Mater. Sci. **55**, 7283–7294 (2020). https://doi.org/10.1007/s10853-020-04518-5